Original Article
J. Korean Wood Sci. Technol. 2022, 50(5): 301-314
https://doi.org/10.5658/WOOD.2022.50.5.301

Journal of the Korean Wood Science and Technology
pISSN: 1017-0715 eISSN: 2233-7180
http://www.woodj.org

Monitoring of Moisture and Dimensional Behaviors of Nail-Laminated Timber (NLT)-Concrete Slab Exposed to Outdoor Air

Sung-Wook HWANG[1] · Hyunwoo CHUNG[2] · Taekyeong LEE[1] · Kyung-Sun AHN[3] · Sung-Jun PANG[1] · Junsik BANG[3] · Hyo Won KWAK[1,2,3] · Jung-Kwon OH[1,2,3] · Hwanmyeong YEO[1,2,3,†]

ABSTRACT

The moisture and dimensional behaviors of a nail-laminated timber (NLT)–concrete slab composed of an NLT–plywood composite and topping concrete are monitored for 385 days. The slab is developed for using as flexural elements such as floors. The humidity control of wood gently introduces significant fluctuations under the ambient relative humidity into the slab, and fluctuations in the relative humidity result in dimensional changes. The equilibrium moisture content of the slab increases from 6.7% to 15.3% during the monitoring period, resulting in a width (radial) strain of 0.58%. The length (longitudinal) strain is negligible, and the height (tangential) strain is excluded from the analysis because of abstruse signal patterns generated. Concrete pouring causes a permanent increase in the width of the NLT–plywood composite. However, the width deforms because the weight of the concrete mixture loosens the nail-laminated structure, not because of the significant amount of moisture in the mixture. The dimensional stabilization effect of the nail-laminated system is demonstrated as the composite strain is lower than the total strain of lumber and plywood, which are elements constituting the nail-laminated structure.

Keywords: monitoring, nail-laminated timber (NLT), strain, wood moisture

1. INTRODUCTION

Advances in timber engineering and prefabrication systems have resulted in the development of mass timber and hence an increase in the number of timber structures (Ahn *et al.*, 2021; Choi *et al.*, 2020, 2021; Eversmann *et al.*, 2017; Fujimoto *et al.*, 2021; Galih *et al.*, 2020; Harte, 2017; Hendrik *et al.*, 2019; Jung *et al.*, 2020; Kremer and Symmons, 2015; Lee *et al.*, 2022; Park *et al.*, 2020; Song and Kim, 2022; Yang *et al.*, 2021). Developing and utilizing novel wood-based structural materials is a practical strategy for realizing the global challenge, “Net Zero by 2050” (Bouckaert *et al.*, 2021). Wood is composed of carbon captured from the atmosphere via photosynthesis during tree growth (De Araujo *et al.*, 2020). Additionally, wood manufacturing consumes

Date Received August 5, 2022, Date Revised August 30, 2022, Date Accepted September 8, 2022
[1] Research Institute of Agriculture and Life Sciences, Seoul National University, Seoul 08826, Korea
[2] Department of Forest Sciences, College of Agriculture and Life Sciences, Seoul National University, Seoul 08826, Korea
[3] Department of Agriculture, Forestry and Bioresources, College of Agriculture and Life Sciences, Seoul National University, Seoul 08826, Korea
[†] Corresponding author: Hwanmyeong YEO (e-mail: hyeo@snu.ac.kr, https://orcid.org/0000-0002-1779-069X)

less fossil fuel than metal, concrete, and plastic products (Bergman *et al*., 2014). Hence, using wood products reduces carbon emission. The "Wood First Act" (British Columbia, 2009) enacted in British Columbia, Canada, and "The Act for Promotion of Use of Wood in Public Buildings" (Japanese Ministry of Agriculture, Forestry, and Fisheries, 2010) enacted in Japan are policies that aim to achieve carbon neutrality by revitalizing the wood industry.

Wood is a hygroscopic material that shrinks and swells repeatedly in response to changes in the surrounding climate (Chang *et al*., 2019; Liu *et al*., 2022; Park and Jo, 2020). Hence, an accurate evaluation of moisture fluctuations caused by changes in ambient air and the consequent dimensional changes must be performed to secure the structural stability of timber structures. Dimensional changes owing to frequent moisture fluctuations cause structural failure in timber structures (Dietsch and Winter, 2018; Franke *et al*., 2015). In addition, damp conditions involving more than 20% moisture content (MC) increase the biodegradation risk of wooden materials (Bobadilha *et al*., 2020; Kirker *et al*., 2016; Sinha *et al*., 2020; Wang *et al*., 2018). Because moisture in wood is a critical factor in determining the stability and lifespan of timber structures, one should perform an accurate diagnosis of moisture changes in wood through monitoring.

Various indirect methods for measuring wood moisture have been reported, such as electrical resistance, radio frequency, and near-infrared spectroscopy (Chang *et al*., 2015; Forsén and Tarvainen, 2000; Nursultanov *et al*., 2017; Reci *et al*., 2016; Yang *et al*., 2015). Among them, electrical resistance methods are preferred for moisture monitoring in timber structures (Björngrim *et al*., 2016; Brischke *et al*., 2008; Dietsch *et al*., 2015a). A four-point probe method based on electrical resistivity has been proposed to compensate for the limitations of electrical resistance affected by the dimensions of a material (Hafsa *et al*., 2021; Hwang *et al*., 2021). Electrical resistance- and resistivity-based methods should account for the tree species, preservatives, stress conditions inside wood due to structural loads, and unstable electrode contacts.

At a specific temperature, wood moisture reaches equilibrium with the surrounding relative humidity (RH), which is known as the equilibrium moisture content (EMC). The sorption equation describes the relationship among the temperature, RH, and EMC (Hailwood and Horrobin, 1946). The large specific surface area of wood allows equilibrium to be attained between the ambient RH and wood moisture rapidly (Mahnert and Hundhausen, 2018). This characteristic renders hygrometric sensors appropriate for monitoring applications (Franke *et al*., 2013).

In this study, the moisture and dimensional changes of a nail-laminated timber (NLT)–plywood composite, which is the base layer for an NLT–concrete hybrid slab developed for effective floor structures, are investigated. NLT, which is used in floors, roofs, shafts, walls, and shear walls, is a mass timber product manufactured by fastening lumber to create a solid structural element from dimensional lumber (Binational Softwood Lumber Council, 2017). Although the structural, mechanical, and fire behaviors of NLT have been evaluated and reported in several studies (Derikvand *et al*., 2019; Herberg, 2018; Hong, 2017; Krämer and Blass, 2001), the moisture and dimensional behaviors are not primary concerns in NLT products. To the best of our knowledge, this study is the first to investigate moisture and dimensional changes in NLT. Investigating the moisture and dimensional behavior of slabs induced by ambient climate change will facilitate in understanding NLT–concrete slabs more comprehensively as well promote the development of reliable monitoring systems.

2. MATERIALS and METHODS

2.1. Slab specimen

2.1.1. Nail-laminated timber (NLT)–plywood composite

The slab used in this study comprises two layers: A lower wooden layer and an upper topping concrete layer. An NLT–plywood composite was used for the wooden layer. The raw material used for the lumber and plywood was Japanese larch wood (*Larix kaempferi*), measuring 24 mm × 140 mm × 1,000 mm (i.e., radial × tangential × longitudinal directions for lumber; thickness × height × length for plywood). All lumber was flat sawn wood or featured an end grain. The air-dry densities of the lumber and plywood were 0.55 and 0.66 g/cm^3, respectively.

As shown in Fig. 1(a), a slab measuring 1,000 mm (width, x-direction) × 140 mm (height, y-direction) × 1,000 mm (length, z-direction) was assembled by repeatedly laminating the elements with screws in the lumber–plywood–lumber sequence. A total of 42 wooden elements, 28 lumbers, and 14 plywood were fastened using coarse thread drywall screws, and the length, head diameter, and shank diameter were 64, 8, and 4.2 mm, respectively. The screws fastened the wooden elements in two rows on the y–z surface of the elements [Fig. 1(d)]. The rows in each layer were arranged alternately.

2.1.2. Topping concrete

An NLT–concrete slab was constructed by placing topping concrete on the NLT–plywood composite (Fig. 2). The nominal strength, nominal maximum size of the coarse aggregate, and slump flow of the ready-mix concrete were 24 MPa, 25 mm, and 120 mm, respectively, and Type I Portland cement was used. The topping con-

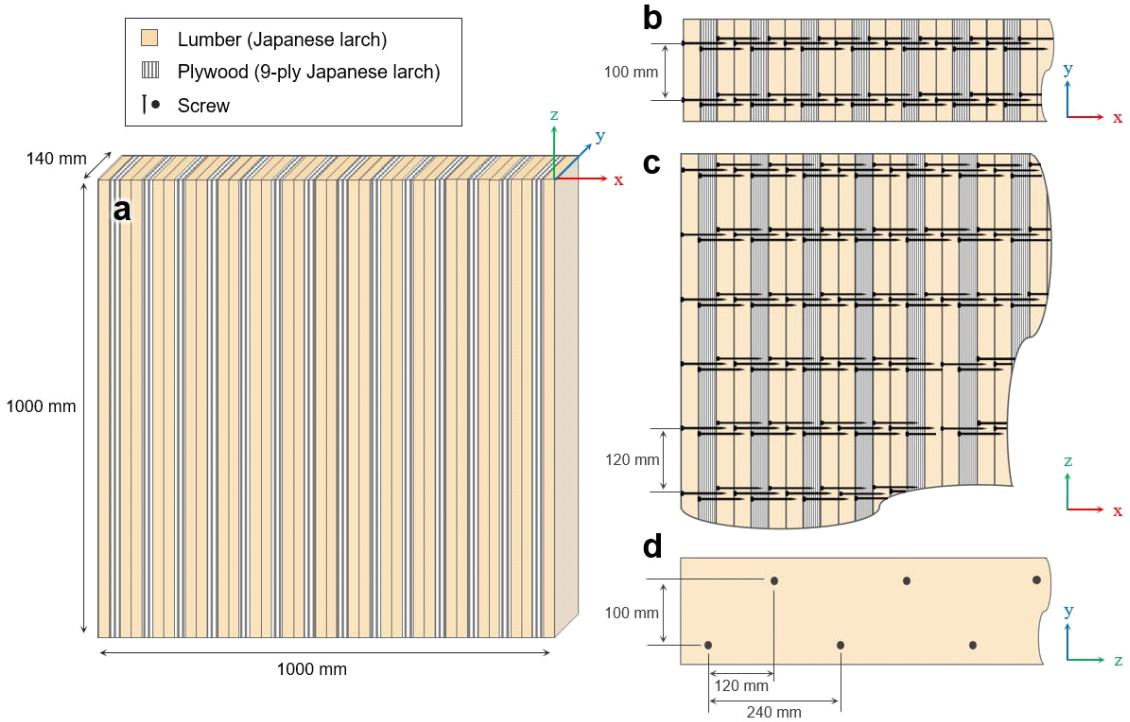

Fig. 1. Schematic diagrams showing the nail-laminated timber–plywood composite. (a) Orthographic view; (b) x–y, (c) x–z, and (d) y–z sections of the composite.

crete was 100 mm thick and unbonded to the underlying NLT.

2.2. Monitoring details

2.2.1. Observation site and period

For long-term monitoring, the slab specimen was placed outdoors (37°45' 79.03' 'N, 126°94'79.62' 'E) at Seoul National University, Gwanak-gu, Seoul. The observation sites were a building on the east side, and a forest and valley on the west side. A canopy was installed over the slab to avoid direct sunlight and prevent rain wetting. The designed monitoring environment was harsher than the actual environment used for the slab. The slab temperature, RH, and dimensional changes were observed from April 14, 2021, to May 3, 2022 (385 d).

2.2.2. Sensors

As illustrated in Fig. 2, type-K thermocouples (TCs) were installed at the bottom of the wooden slab to measure the internal temperature. Cavities with a diameter of 2 mm and depth of 70 mm were drilled at nine points in the bottom quadrant, and the TCs were inserted into the cavities. The gaps between the TCs and wooden slabs were sealed with polyvinyl acetate (PVA) adhesive to prevent temperature changes due to the inflow of outside air.

Two thermo-hygrometers (HMP 60, Vaisala, Vantaa, Finland) were installed to measure the temperature and RH of the wooden slab and the external air. The sensor used for the slab was inserted at a depth of 70 mm and was double sealed using PVA adhesive and silicone sealant in the center of the slab bottom; meanwhile, the sensor for air was placed in an instrument shelter.

The dimensional change in the slab was measured using three wire tension-type displacement transducers (DP-500G, Tokyo Measuring Instruments Laboratory, Tokyo, Japan) installed in the slab surface width (x), height (y), and length (z) directions. The details of the sensors used to monitor the slab are listed in Table 1.

2.2.3. Real-time monitoring and data acquisition

The data generated from the sensors installed in the NLT–plywood composite were controlled using a data

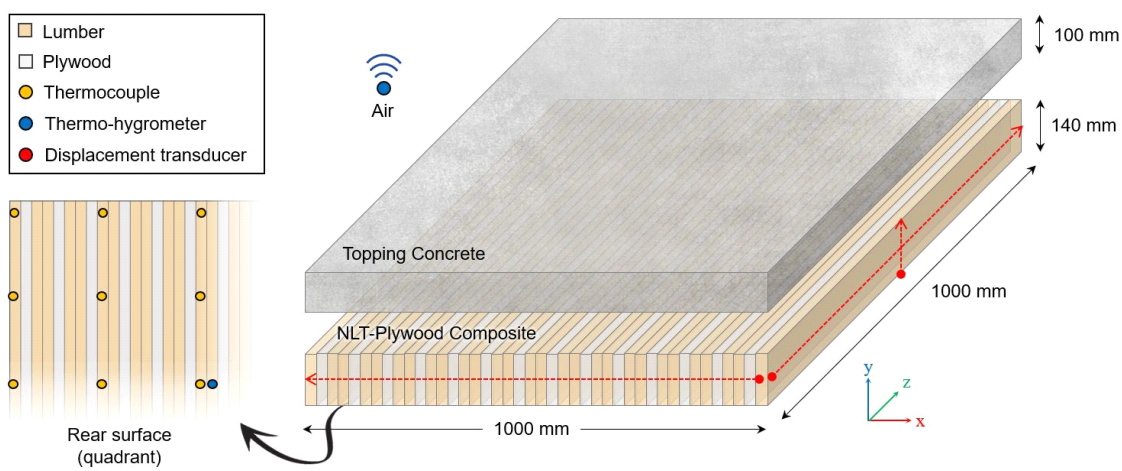

Fig. 2. Schematic diagram showing the NLT–concrete slab and installation position of sensors. NLT: nail-laminated timber.

Table 1. Details of sensors used for monitoring temperature, RH, and displacement

Element	Period (YY/MM/DD)	Sensor (quantity)	Position
Temp.	21/04/13 to 22/05/03	Type-K thermocouple (9)	Slab (inside)
Temp. & RH	21/04/13 to 22/05/03	Thermo-hygrometer (2)	Slab (inside) / Air (outdoor)
Displacement	21/05/28 to 22/05/03	Displacement transducer (3)	Slab (surface)

Temp.: temperature, RH: relative humidity.

logger (CR3000, Campbell Scientific, Logan, UT, USA) equipped with a relay multiplexer (AM16/32B, Campbell Scientific). All sensors provided measurements for each target at 30 s intervals, and the dedicated data logger software provided real-time sensor data monitoring. Average values provided by the TCs, thermo-hygrometers, and displacement transducers for 30 min and 24 h were acquired from the data logger and used to analyze the temperature, RH, and dimensional changes of the slab.

2.3. Evaluation of moisture and dimensional changes

2.3.1. Equilibrium moisture content (EMC)

The EMC was calculated using the temperature and RH data from the thermo-hygrometer sensors to evaluate the change in moisture inside the slab. The Hailwood–Horrobin equation (Hailwood and Horrobin, 1946) was employed to calculate the EMC, as follows:

$$EMC = \frac{1800}{W} \times \left(\frac{kh}{1-kh} + \frac{k_1 kh + 2k_1 k_2 k^2 h^2}{1 + k_1 kh + k_1 k_2 k^2 h^2} \right) \quad (1)$$

$$W = 349 + 1.29T + 0.0135T^2$$
$$k = 0.805 + 0.000736T - 0.00000273T^2$$
$$k_1 = 6.27 - 0.00938T - 0.000303T^2$$
$$k_2 = 1.91 + 0.0407T - 0.000293T^2$$

where T is the temperature in Celsius; h is the RH (%); W, k, k_1, and k_2 are the fundamental constants of the Hailwood–Horrobin sorption model.

2.3.2. Strain

Moisture fluctuations in the NLT slab result in dimensional changes. The displacement values in the x-, y-, and z-directions were converted into strain values using the following equation to measure the dimensional change of the slab:

$$\epsilon = \frac{l_d - l_i}{l_i} \times 100 \ (\%), \quad (2)$$

where ε is the strain, l_i the initial length, and l_d the deformed length of the NLT slab.

EMC fluctuation-induced strains were calculated using the reference shrinkage of Japanese larch wood (Kim and Lee, 2002; Park *et al*., 2015) based on the measured shrinkage of plywood to investigate the effect of the nail-laminated structure on dimensional change. Because the slab was a laminated structure composed of lumber and plywood, the calculated strain in the x-direction (width) was weighted for each element, as follows:

$$\epsilon_{\%S} = \left(\epsilon_{\%L} \times \left(\frac{N_L}{N_T} \right) \right) + \left(\epsilon_{\%P} \times \left(\frac{N_P}{N_T} \right) \right), \quad (3)$$

where $\varepsilon_{\%S}$, $\varepsilon_{\%L}$, and $\varepsilon_{\%P}$ are the strains per 1% MC of the slab, lumber, and plywood, respectively, below the fiber saturation point; N_L and N_P are the number of lumber and plywood elements constituting the slab, respectively; N_T is the total number of elements. The cal-

culated strains were compared with the strains measured using displacement transducers.

3. RESULTS and DISCUSSION

3.1. Climate of observation site

Fig. 3 shows a comparison of the temperature and RH at the observation site with those of Seoul during the same period. The daily temperature fluctuation at the observation site showed a trend similar to that of Seoul. The mean temperature in the area during the monitoring period was 13.4℃, which is equivalent to 13.5℃ in Seoul. However, the RH of the observation site was higher than that of Seoul and indicated more significant fluctuations. As shown in the subplots in Fig. 3, the observation site experienced a more humid climate than the reference area of Seoul in the summer. The mean and standard deviation of the RH at the observation site during the monitoring period were 70.4% and 18.4, respectively, which were higher than the reference values of 64.8% and 13.2, respectively. Forests and valleys in the vicinity may have affected the wet environment of the observation site.

3.2. Temperature and relative humidity (RH) changes

3.2.1. Temperature

The internal temperature of the NLT slab, as acquired using the TCs, reflected the air temperature. The speed at which the air temperature affected the slab differed depending on the TC location. The TCs at the edge of the slab (TC1, TC2, TC3, TC4, and TC7 in Fig. 4) recorded temperatures similar to the air temperature, with a time difference of 60 min. Meanwhile, the TCs near the center (TC5, TC6, TC8, and TC9 in Fig. 4) recorded temperatures similar to the air temperature at intervals of 90–120 min. The TC position affected the range of temperature fluctuation. Based on the subplot shown in Fig. 4, the temperature recorded by the five TCs located at the edge of the slab showed more significant changes

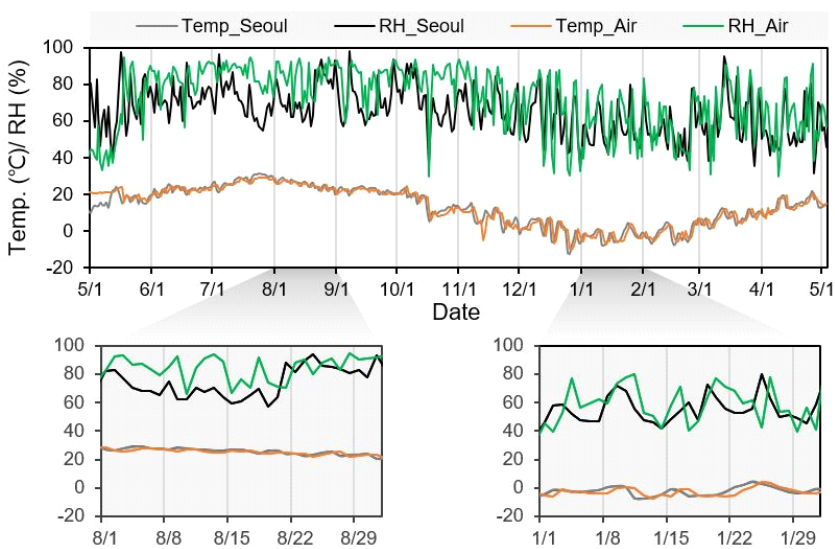

Fig. 3. Changes in temperature and RH at the observation site and comparison with data measured at the Seoul Weather Station. RH: relative humidity.

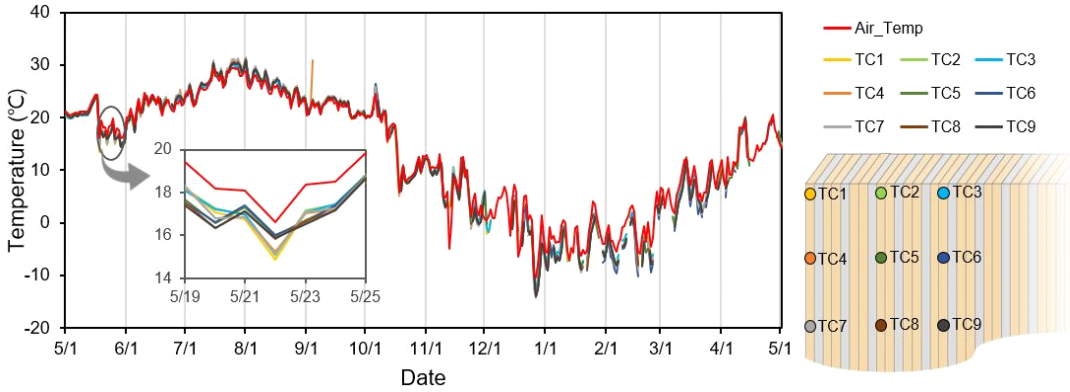

Fig. 4. Internal temperature changes of the slab due to change in air temperature.

than that by the four TCs inside, resulting in the formation of two clusters.

3.2.2. Relative humidity (RH) and equilibrium moisture content (EMC)

Table 2 lists the descriptive statistics of the data obtained from the external air and the slab. In contrast to the temperature change, the RH fluctuation of the air was not directly reflected in the internal RH of the NLT slab, and the fluctuation reduced significantly [Fig. 5(a)]. Naturally, the change in the air RH would change the internal RH of the slab. However, the internal RH fluctuations were much gentler, which was due to the damping and delayed adaptation of moisture (Dietsch *et al*., 2015b). The mild RH change in the NLT slab was attributed to the humidity control of the wood material.

Fig. 5(b) shows the EMC of the air and NLT slabs calculated using the Hailwood–Horrobin equation. The changes in the EMC reflected the fluctuation pattern of the RH. This is because RH is a critical factor that determines the EMC. During the monitoring period, when the air EMC fluctuated in the range of 6.2%–24%, the EMC change in the slab was 6.7%–15.3% (Table 2). The high MC of wood, i.e., exceeding 20%, would deteriorate the strength and biodegradation of the slabs (Kirker *et al*., 2016; Shupe *et al*., 2008). However, such defects are unlikely to occur within the internal EMC range of the slab investigated in this study.

The effect of concrete pouring on moisture change in the NLT slab was negligible. The slight increase in the internal RH and EMC of the slab observed immediately after pouring concrete (October 5, 2021) was due to the increase in the air RH, not the moisture in the concrete mixture (Fig. 5). This is because the internal moisture

Table 2. Descriptive statistics of data acquired from air and the NLT slab

Station	N	Temperature (℃)					RH (%)					EMC (%)				
		Min.	Max.	Range	Mean	SD	Min.	Max.	Range	Mean	SD	Min.	Max.	Range	Mean	SD
Air	385	−10.4	29.5	39.8	13.4	10.4	29.6	94.8	65.2	70.4	18.4	6.2	24.0	17.8	14.6	4.7
Slab	385	−9.6	30.2	39.8	13.8	10.3	33.1	77.2	44.2	64.5	11.0	6.7	15.3	8.6	12.2	2.2

NLT: nail-laminated timber, N: number of data points, Min.: minimum, Max.: maximum, SD: standard deviation, RH: relative humidity, EMC: equilibrium moisture content.

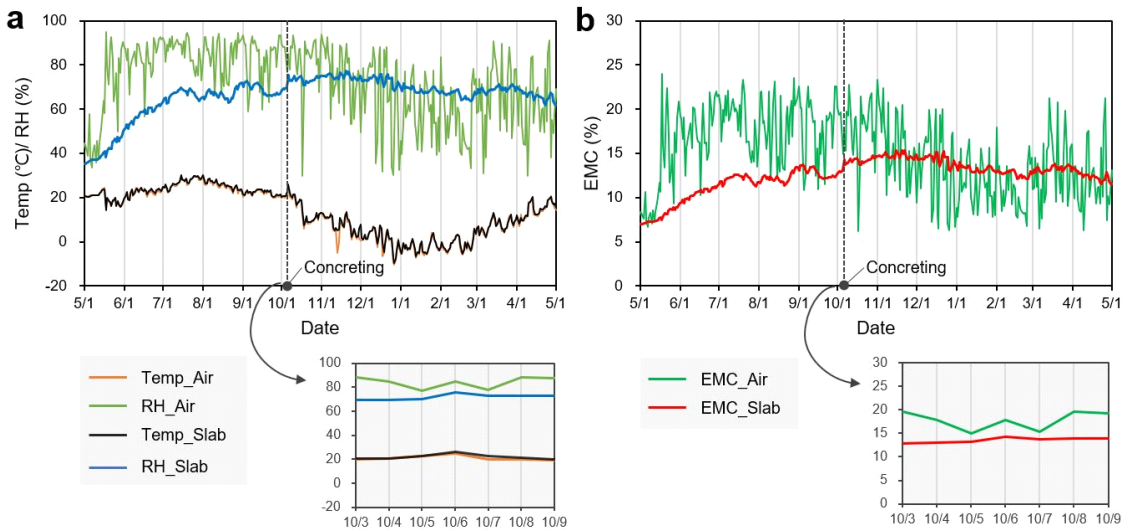

Fig. 5. Plots showing internal moisture change in the NLT slab measured using thermo-hygrometers. (a) Internal temperature and RH fluctuations, (b) EMC fluctuations. EMC: equilibrium moisture content, NLT: nail-laminated timber, RH: relative humidity.

of the slab did not increase continuously after concrete pouring and reflected the air RH fluctuations [subplots in Fig. 5(a) and (b)]. These results indicate that concrete pouring is not a significant factor in increasing the internal moisture of the slab.

3.3. Dimensional change

Table 3 and Fig. 6 show the linear dimensional changes in the width, height, and length directions induced by the changes in the internal moisture of the NLT–plywood composite. The changes in the width and length were the most and least significant, respectively (Table 3). The patterns of dimensional change in the three directions were similar to those of the internal EMC fluctuation of the slab (Fig. 6).

The internal EMC at the end of the observation was higher than that at the beginning; hence, volume swelling of the slab was expected. However, the width and length increased, whereas the height decreased. Because flat-sawn wood was used as the lumber element of the NLT–plywood composite, the height of the latter cor-

Table 3. Descriptive statistics of displacement data acquired from the NLT slab

Structural direction	N	Displacement (mm)					Strain (%)				
		Min.	Max.	Range	Mean	SD	Min.	Max.	Range	Mean	SD
Width (x)	385	−0.07	5.46	5.52	3.53	1.82	−0.007	0.574	0.582	0.371	0.191
Height (y)	385	−0.27	0.20	0.46	−0.08	0.10	−0.190	0.142	0.332	−0.058	0.068
Length (z)	385	−0.37	0.81	1.18	0.24	0.31	−0.038	0.085	0.124	0.025	0.033

NLT: nail-laminated timber, N: number of data points, Min.: minimum, Max.: maximum, SD: standard deviation.

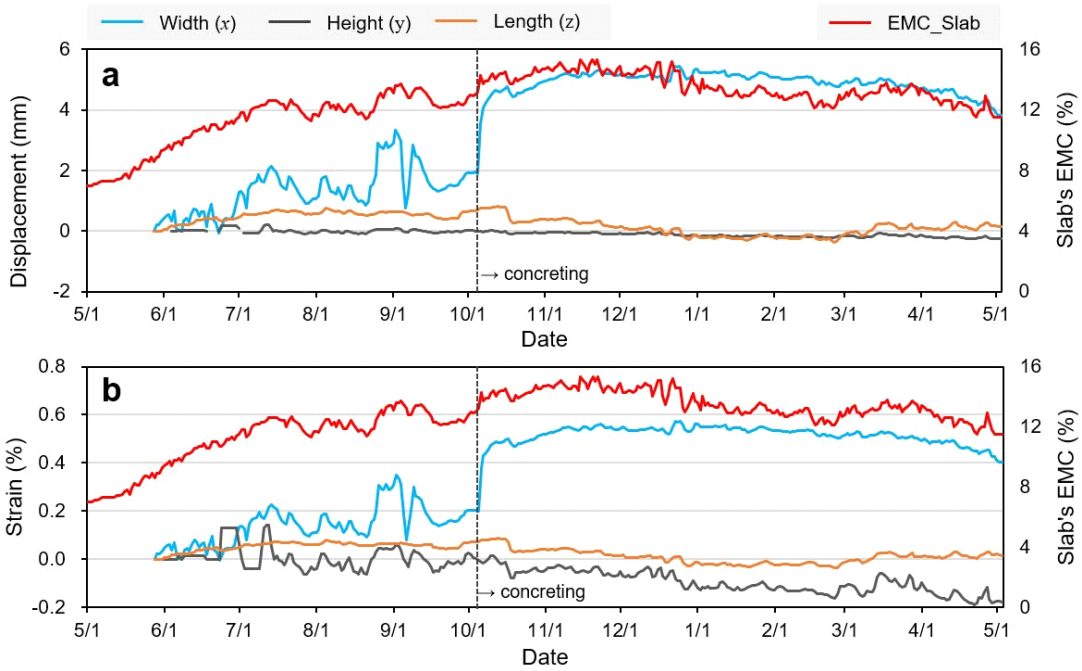

Fig. 6. Fluctuations in displacement (a) and strain (b) in three directions due to internal EMC change of the NLT slab. EMC: equilibrium moisture content, NLT: nail-laminated timber.

responded to the tangential direction. Considering the shrinkage and swelling anisotropy of wood, the dimensional change in the tangential direction should be greater than those in the radial and longitudinal directions. Therefore, a decrease in the height direction is difficult to interpret theoretically. The displacement transducer installed in the height direction caused the wire to bent 90° relative to its typical travel path by pulleys installed on a narrow surface. It appears that the artificial change in the wire travel path generated unexplained displacements in the height direction. Therefore, the height direction was not considered in the dimensional change analysis.

The internal EMC of the slab, which increased continuously since the monitoring began, reached a maximum value of 15.3% on November 22 and started declining as winter approached. Accordingly, the slab width changed as well (Fig. 6). However, the length strain was extremely small, i.e., approximately zero [Fig. 6(b)]. The acute swelling in the width caused by concrete pouring, as shown in Fig. 6(a) and (b), is noteworthy. After the concrete was poured, the width strain increased by 0.23%. This significant deformation was irreversible and permanent, as it did not recover during the subsequent internal EMC reduction phase. As mentioned earlier, concrete pouring did not increase the internal moisture of the slab. Therefore, the width deformation was likely due to external factors, such as the loosening of the nail lamination due to the load of the concrete mixture. The nail-laminated system implies low resistance in the lamination direction (Binational Softwood Lumber Council, 2017).

Table 4 shows the calculated radial strains of the lumber and the thickness strains of the plywood corres-

Table 4. Radial strains of the NLT slab and its elements

Component	EMC (%)		Strain (%)	Strain/%EMC	Reference
	Min.	Max.			
NLT slab (measured)	8.9	15.3	0.53	0.083	-
Before concreting	8.9	13.7	0.33	0.068	-
After concreting	11.5	15.3	0.15	0.041	-
NLT slab (calculated)	-	-	-	0.136	-
Lumber	0	16.0	2.09	0.142[1)]	Kim and Lee (2002)
	0	10.8	1.64		Park *et al.* (2015)
Plywood	6.3	13.3	0.88	0.126[2)]	Measured

[1)] Average of reported shrinkages from both references.
[2)] Thickness strain.
NLT: nail-laminated timber, EMC: equilibrium moisture content, Min.: minimum, Max.: maximum, Strain/%EMC: strain per 1% EMC.

ponding to the width strain of the NLT slab. Comparing the calculated and measured values of the width deformation, the strain per 1% change in the EMC measured by the displacement transducer was 0.83%, which is approximately 39% lower than the calculated strain of 0.136% (Table 4). The low measured strain was attributed to the suppression of dimensional changes by the nail-laminated structure, as well as the restraining effect caused by the load of the concrete topping.

Fig. 7 shows plots of the measured and calculated strains in the width direction. Although the measured values were lower than the calculated values, the variation patterns of both were similar. Near the monitoring end, the measured and calculated strains were reversed, which implies that the significant increase in the width due to concrete pouring was permanent. The variation in the measured strain after concrete pouring reduced significantly. The strain per 1% of EMC decreased from 0.068% to 0.041% after concrete placement (Table 4). These results suggest that the nail lamination structure

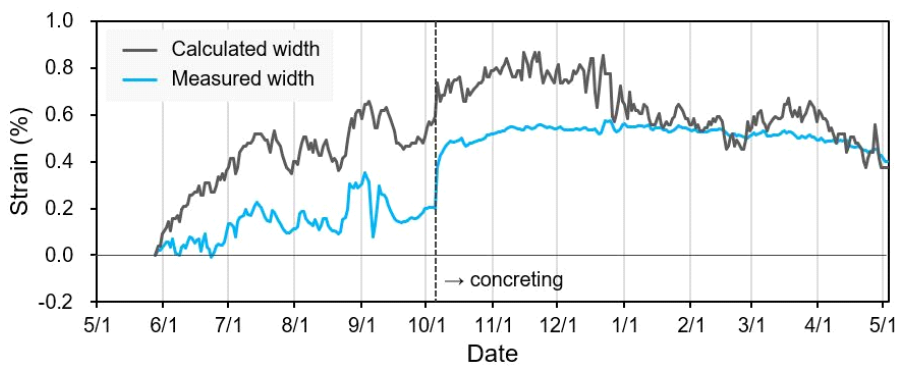

Fig. 7. Comparison of strains based on measured and calculated widths of the NLT slab. NLT: nail-laminated timber.

loosened because of concrete pouring. This is because the space created by the loose nail-laminated structure offset the actual dimensional change of the composite elements.

Dimensional changes are critical to structural stability. In this study, the NLT–concrete slab was lifted from the ground throughout the monitoring period to ensure smooth shrinkage and swelling. This experimental design may have loosened the nail-laminated structure. At timber construction sites, such permanent changes in dimensions are expected to be reduced using beams to support the lower section of the slab.

The monitoring of the improved slab using more precise sensors that can compensate for the technical limitations of this study is in progress. Subsequent studies will be performed to investigate the effects of the base NLT and topping concrete slabs on moisture and dimensional changes.

4. CONCLUSIONS

The change in air temperature was almost directly reflected in the internal temperature of the NLT–plywood composite. By contrast, the change in RH was moderate because the humidity of wood was controlled. During the monitoring period of 385 d, the internal EMC of the composite fluctuated within the range of 6.7%–15.3%, and the change in moisture resulted in dimensional change. Concrete pouring did not substantially affect the internal moisture of the composite, and the nail-laminated structure suppressed dimensional change. The dimensional stability of the designed NLT–plywood composite was demonstrated by its dimensional change, which was less than that of each of its constituent element.

CONFLICT of INTEREST

No potential conflict of interest relevant to this article was reported.

ACKNOWLEDGMENT

This study was supported by the Korea Forestry Promotion Institute through the R&D Program for Forest Science Technology funded by the Korea Forest Service (Project No. 2020224C10-2022-AC02).

REFERENCES

Ahn, K.S., Pang, S.J., Oh, J.K. 2021. Prediction of withdrawal resistance of single screw on Korean wood products. Journal of the Korean Wood Science and Technology 49(1): 93-102.

Bergman, R., Puettmann, M., Taylor, A., Skog, K.E. 2014. The carbon impacts of wood products. Forest Products Journal 64(7-8): 220-231.

Binational Softwood Lumber Council. 2017. Nail-laminated timber U. S. design & construction guide. https://sweets.construction.com/swts_content_files/153333/3309087.pdf

Björngrim, N., Hagman, O., Wang, X.A. 2016. Moisture content monitoring of a timber footbridge. BioResources 11(2): 3904-3913.

Bobadilha, G.S., Stokes, C.E., Kirker, G., Ahmed, S.A., Ohno, K.M., Lopes, D.J.V. 2020. Effect of exterior wood coatings on the durability of cross-laminated timber against mold and decay fungi. BioResources 15(4): 8420-8433.

Bouckaert, S., Pales, A.F., McGlade, C., Remme, U., Wanner, B., Varro, L., D'Ambrosio, D., Spencer, T. 2021. Net Zero by 2050: A Roadmap for the Global Energy Sector. International Energy Agency, Paris, France.

Brischke, C., Rapp, A.O., Bayerbach, R. 2008. Measurement system for long-term recording of wood moisture content with internal conductively glued electrodes. Building and Environment 43(10): 1566-

1574.

British Columbia. 2009. Wood first act. https://www.bclaws.gov.bc.ca/civix/document/id/complete/statreg/09018_01

Chang, Y.S., Han, Y., Eom, C.D., Jeon, S., Yeo, H. 2019. Hygroscopic property of heat treated yellow poplar (*Liriodendron tulipifera*) wood. Journal of the Korean Wood Science and Technology 47(6): 761-769.

Chang, Y.S., Yang, S.Y., Chun, H., Kang, K.Y., Choi, J.W., Choi, I.G., Yeo, H. 2015. Development of moisture content prediction model for *Larix kaempferi* sawdust using near infrared spectroscopy. Journal of the Korean Wood Science and Technology 43(3): 304-310.

Choi, G.W., Yang, S.M., Lee, H.J., Kim, J.H., Choi, K.H., Kang, S.G. 2020. A study on the block shear strength according to the layer composition of and adhesive type of ply-lam CLT. Journal of the Korean Wood Science and Technology 48(6): 791-806.

Choi, G.W., Yang, S.M., Lee, H.J., Kim, J.H., Choi, K.H., Kang, S.G. 2021. Evaluation of flexural performance according to the plywood bonding method of ply-lam CLT. Journal of the Korean Wood Science and Technology 49(2): 107-121.

De Araujo, V., Vasconcelos, J., Cortez-Barbosa, J., Morales, E., Christoforo, A., Gava, M., Lahr, F., Garcia, J. 2020. Wood consumption and fixations of carbon dioxide and carbon from timber housing techniques: A Brazilian panorama. Energy and Buildings 216:109960.

Derikvand, M., Jiao, H., Kotlarewski, N., Lee, M., Chan, A., Nolan, G. 2019. Bending performance of nail-laminated timber constructed of fast-grown plantation eucalypt. European Journal of Wood and Wood Products 77(3): 421-437.

Dietsch, P., Franke, S., Franke, B., Gamper, A., Winter, S. 2015a. Methods to determine wood moisture content and their applicability in monitoring concepts. Journal of Civil Structural Health Monitoring 5(2): 115-127.

Dietsch, P., Gamper, A., Merk, M., Winter, S. 2015b. Monitoring building climate and timber moisture gradient in large-span timber structures. Journal of Civil Structural Health Monitoring 5(2): 153-165.

Dietsch, P., Winter, S. 2018. Structural failure in large-span timber structures: A comprehensive analysis of 230 cases. Structural Safety 71: 41-46.

Eversmann, P., Gramazio, F., Kohler, M. 2017. Robotic prefabrication of timber structures: Towards automated large-scale spatial assembly. Construction Robotics 1: 49-60.

Forsén, H., Tarvainen, V. 2000. Accuracy and Functionality of Hand Held Wood Moisture Content Meters. VTT Technical Research Centre of Finland, Espoo, Finland.

Franke, B., Franke, S., Müller, A. 2015. Case studies: Long-term monitoring of timber bridges. Journal of Civil Structural Health Monitoring 5(2): 195-202.

Franke, B., Franke, S., Müller, A., Vogel, M., Scharmacher, F., Tannert, T. 2013. Long term monitoring of timber bridges: Assessment and results. Advanced Materials Research 778: 749-756.

Fujimoto, Y., Tanaka, H., Morita, H., Kang, S.G. 2021. Development of ply-lam composed of Japanese cypress laminae and Korean larch plywood. Journal of the Korean Wood Science and Technology 49(1): 57-66.

Galih, N.M., Yang, S.M., Yu, S.M., Kang, S.G. 2020. Study on the mechanical properties of tropical hybrid cross laminated timber using bamboo laminated board as core layer. Journal of the Korean Wood Science and Technology 48(2): 245-252.

Hafsa, W., Angellier, N., Takarli, M., Pop, O. 2021. A mixed experimental–numerical electrical resistivity-based method for moisture content assessment in wood tested using the example of Douglas fir. Wood Science and Technology 55(3): 697-718.

Hailwood, A.J., Horrobin, S. 1946. Absorption of water by polymers: Analysis in terms of a simple model. Transactions of the Faraday Society 42: B084-B092.

Harte, A.M. 2017. Mass timber − The emergence of a modern construction material. Journal of Structural Integrity and Maintenance 2(3): 121-132.

Hendrik, J., Hadi, Y.S., Massijaya, M.Y., Santoso, A., Pizzi, A. 2019. Properties of glued laminated timber made from fast-growing species with mangium tannin and phenol resorcinol formaldehyde adhesives. Journal of the Korean Wood Science and Technology 47(3): 253-264.

Herberg, E. 2018. Flexural performance of nail-laminated timber crane mats. Ph.D. Thesis, University of Minnesota, USA.

Hong, K.E.M. 2017. Structural performance of nail-laminated timber-concrete composite floors. Ph.D. Thesis, University of British Columbia, Canada.

Hwang, S., Hwang, S., Lee, T., Ahn, K., Pang, S., Park, J., Oh, J., Kwak, H., Yeo, H. 2021. Investigation of electrical characteristics using various electrodes for evaluating the moisture content in wood. BioResources 16(4): 7040-7055.

Japanese Ministry of Agriculture, Forestry, and Fisheries. 2010. The act for promotion of use of wood in public buildings, etc. https://elaws.e-gov.go.jp/document?lawid=422AC0000000036_20211001_503AC0000000077

Jung, H., Song, Y., Hong, S. 2020. Effect of glass fiber-reinforced connection on the horizontal shear strength of CLT walls. Journal of the Korean Wood Science and Technology 48(5): 685-695.

Kim, J.H., Lee, W.H. 2002. Physical properties of larch (*Larix kaemferi* Carr.) treated by high temperature steaming-Effect of high temperature steaming on shrinkages of larch block. Journal of the Korean Wood Science and Technology 30(2): 102-107.

Kirker, G.T., Bishell, A.B., Zelinka, S.L. 2016. Electrical properties of wood colonized by *Gloeophyllum trabeum*. International Biodeterioration & Biodegradation 114:110-115.

Krämer, V., Blass, H. 2001. Load carrying capacity of nail-laminated timber under concentrated loads. In: Venice, Italy, Proceedings of the 34th CIB W18 Meeting, pp. 22-24.

Kremer, P.D., Symmons, M.A. 2015. Mass timber construction as an alternative to concrete and steel in the Australia building industry: A PESTEL evaluation of the potential. International Wood Products Journal 6(3): 138-147.

Lee, I.H., Kim, K., Shim, K. 2022. Evaluation of bearing strength of self-tapping screws according to the grain direction of domestic *Pinus densiflora*. Journal of the Korean Wood Science and Technology 50(1): 1-11.

Liu, J., Ji, Y., Lu, J., Li, Z. 2022. Mechanical behavior of treated timber boardwalk decks under cyclic moisture changes. Journal of the Korean Wood Science and Technology 50(1): 68-80.

Mahnert, K.C., Hundhausen, U. 2018. A review on the protection of timber bridges. Wood Material Science & Engineering 13(3): 152-158.

Nursultanov, N., Altaner, C., Heffernan, W.J.B. 2017. Effect of temperature on electrical conductivity of green sapwood of *Pinus radiata* (radiata pine). Wood Science and Technology 51(4): 795-809.

Park, H.J., Jo, S.U. 2020. Moisture absorption and desorption properties of Douglas fir, hinoki, larch, plywood, and WML board® in response to humidity variation. Journal of the Korean Wood Science and Technology 48(4): 488-502.

Park, J., Song, Y., Hong, S. 2020. Bending creep of glulam and bolted glulam under changing relative humidity. Journal of the Korean Wood Science and Technology 48(5): 676-684.

Park, Y., Han, Y., Park, J.H., Chang, Y.S., Yang, S.Y., Chung, H., Kim, K., Yeo, H. 2015. Evaluation of physico-mechanical properties and durability of

Larix kaempferi wood heat-treated by hot air. Journal of the Korean Wood Science and Technology 43(3): 334-343.

Reci, H., Maï, T.C., Sbartaï, Z.M., Pajewski, L., Kiri, E. 2016. Non-destructive evaluation of moisture content in wood using ground-penetrating radar. Geoscientific Instrumentation, Methods and Data Systems 5(2): 575-581.

Shupe, T., Lebow, S., Ring, D. 2008. Causes and Control of Wood Decay, Degradation & Stain. Louisiana State University, Agricultural Center, Baton Rouge, LA, USA.

Sinha, A., Udele, K.E., Cappellazzi, J., Morrell, J.J. 2020. A method to characterize biological degradation of mass timber connections. Wood and Fiber Science 52(4): 419-430.

Song, D., Kim, K. 2022. Influence of manufacturing environment on delamination of mixed cross laminated timber using polyurethane adhesive. Journal of the Korean Wood Science and Technology 50(3): 167-178.

Wang, J.Y., Stirling, R., Morris, P.I., Taylor, A., Lloyd, J., Kirker, G., Lebow, S., Mankowski, M., Barnes H.M., Morrell J.J. 2018. Durability of mass timber structures: A review of the biological risks. Wood and Fiber Science 50: 110-127.

Yang, S.M., Lee, H.H., Kang, S.G. 2021. Research trends in hybrid cross-laminated timber (CLT) to enhance the rolling shear strength of CLT. Journal of the Korean Wood Science and Technology 49(4): 336-359.

Yang, S.Y., Han, Y., Park, J.H., Chung, H., Eom, C.D., Yeo, H. 2015. Moisture content prediction model development for major domestic wood species using near infrared spectroscopy. Journal of the Korean Wood Science and Technology 43(3): 311-319.